ChemPubSoc Europe

DOI: 10.1002/cphc.201500548

CHEMPHYSCHEM Articles

On the Resolution Limit of Femtosecond Stimulated Raman Spectroscopy: Modelling Fifth-Order Signals with Overlapping Pulses

Giuseppe Fumero,[a] Giovanni Batignani,[a, b] Konstantin E. Dorfman,[c] Shaul Mukamel,[a] and Tullio Scopigno*[a, d]

Femtosecond stimulated Raman scattering (FSRS) spectroscopy is a powerful pump–probe technique that can track electronic and vibrational dynamics with high spectral and temporal resolution. The investigation of extremely short-lived species, however, implies deciphering complex signals and is ultimately hampered by unwanted nonlinear effects once the time resolution limit is approached and the pulses overlap temporally. Using the loop diagrams formalism we calculate the fifth-order response of a model system and address the limiting case where the relevant dynamics timescale is comparable to the pump–pulse duration and, consequently, the pump and the probe overlap temporally. We find that in this regime, additional diagrams that do not contribute for temporally well separated pulses need to be taken into account, giving rise to new time-dependent features, even in the absence of photoinduced dynamics and for negative delays.

1. Introduction

The understanding of many physical, chemical and biological systems often requires the investigation of ultrafast dynamical processes with high precision. Spontaneous Raman (SR) spectroscopy is a powerful tool, endowed with structural sensitivity, able to probe Raman-active system dynamics in time-resolved experiments.[1,2] In this technique, the spectral and temporal resolutions are restricted by the fundamental Fourier transform limit,[3] making time-resolved SR spectroscopies not suitable for the study of sub-picosecond dynamics. The development of nonlinear optical techniques has allowed the introduction of femtosecond stimulated Raman scattering (FSRS) spectroscopy[4,5] as a tool for studying ultrafast processes,[6–9] providing improved spectral and temporal resolution.[5,10–12]

FSRS is a six-wave mixing technique, hence it requires five light–matter interactions. The process starts with a femtosecond actinic pump (AP) pulse E_a to photoexcite the system and trigger the dynamics of interest, for example, promoting a vibrational wavepacket in an electronic excited level. Then, after a tunable delay time T, the joint action of a narrowband Raman pulse (RP) E_p and an ultrashort white light continuum probe pulse (PP) E_s allows the detection of molecular vibrations via stimulated Raman scattering.

[a] G. Fumero, G. Batignani, Prof. S. Mukamel, Prof. T. Scopigno
Dipartimento di Fisica, Universitá di Roma "La Sapienza", I-00185, Roma (Italy)
E-mail: tullio.scopigno@phys.uniroma1.it

[b] G. Batignani
Dipartimento di Scienze Fisiche e Chimiche, Universitá degli Studi dell'Aquila, I-67100, L'Aquila (Italy)

[c] Dr. K. E. Dorfman
Department of Chemistry, University of California, California 92697-2025, Irvine (USA)

[d] Prof. T. Scopigno
Center for Life Nano Science @Sapienza, Istituto Italiano di Tecnologia, 295 Viale Regina Elena, I-00161, Roma (Italy)

In the last years, the very issue of the actual time resolution limit of this technique has been the focus of an interesting debate.[3,13,14] Since the vibrational coherences can be induced with a time precision independent on the pulses' bandwidth, it has been argued that FSRS may transcend the usual restrictions, which compromises time and energy resolution in conventional SR time-resolved spectroscopy.[15,16] However, it has been pointed out that when the dynamics of interest are faster that the vibrational dephasing time, signals are far more complex than in ordinary time-resolved spontaneous Raman, and data interpretation has to be supported by rigorous modeling to achieve a real improvement of the time resolution.[14,17,18] Bearing this caveat in mind, the ultimate resolution of the FSRS process is under debate, as one may be tempted to explore the extreme case of temporally overlapped pump and probe pulses.

Generally, n-wave mixing processes are described by a semiclassical approach, in which the matter degrees of freedom, treated quantum-mechanically, interact with classical fields. All possible contributions to the nonlinear signal are accounted for through diagrammatic techniques. Double-sided (ladder) Feynman diagrams provide the fully time ordered description of the density matrix evolution during the nonlinear process.[19] When the order of the process is high, the calculation requires extensive computational efforts, due to the huge number of possible ordering between the fields, the number of possible diagrams, which scales quadratically with n. In many cases, the number of diagrams is reduced by experimental conditions. In particular, in the pump probe scheme, diagrams in which the pump pulse comes after the probe may be neglected.

In a typical FSRS experiment, the pump–probe description holds: the time delay T is scanned in steps larger than the temporal widths of the two ultrashort pulses E_a and E_s. The nonlinear signal is then mainly generated outside the temporal

region in which the E_a and E_s pulses overlap. The number of diagrams needed to compute the signal is significantly reduced to the ones in which the temporally first interactions are with the E_a field.

However, when detecting extremely short-lived dynamics,[20] the characteristic evolution time can be comparable to the temporal widths of the pulses used to monitor it. The nonlinear signal is then almost exclusively generated in the overlap region between the pulses and, consequently, all possible orderings between the fields must be considered.

In this paper, we address the issue of the ultimate FSRS time resolution. To this aim, we calculate the FSRS signal in the pulse overlap regime by means of loop diagrams.[21] The number of such diagrams scales linearly with the nonlinearity order, reducing the number of contributions and the computational effort.[22] The matter and field degrees of freedom, coupled during the nonlinear interaction, are described through the evolution of the wave function ψ, intuitively depicted by the loop diagrams. To isolate the possible presence of unwanted non linear effects which could hamper the detection of the desired dynamics, we assume an actinic pump which does not generate any photoinduced dynamics, evaluating the fifth order response for an electronically off-resonant system.

2. Theoretical Framework

The FSRS process is described by the Hamiltonian [Eq. (1)]:

$$H = H_0 + H_F + H' \tag{1}$$

which includes a contribution from the matter and the field degrees of freedom, H_0 and H_F, respectively, as well as an interaction term H'. We assume that all pulses are far from the resonance frequencies of the sample. This allows us to exclude all the contributions generated by the actinic pump absorption and then to verify the effects not related to the photoinduced dynamics in the sample. The effective radiation–matter interaction Hamiltonian in the rotating wave approximation (RWA) is given by Equation (2):

$$H'(t) = \alpha(t) \sum_{i,j} \mathcal{E}_j^\dagger(t)\mathcal{E}_i(t) + h.c. \tag{2}$$

where $\alpha = \sum_{a\neq b} \alpha_{ab}|a\rangle\langle b|$ is the excited-state polarizability, i and j run over the modes of the three fields and $\mathcal{E}_j = \left(\frac{\hbar\omega_j}{2\epsilon_0 V}\right)^{\frac{1}{2}} \hat{a}_j e^{-i\omega_j t}$ and $\mathcal{E}_j^\dagger$ are the positive and negative frequency components of the field operator for mode j [Eq. (3)]:

$$\hat{E}(\mathbf{r},t) = \sum_j \mathcal{E}_j(t)e^{i\mathbf{k_j}\cdot\mathbf{r}} + \sum_j \mathcal{E}_j^\dagger(t)e^{-i\mathbf{k_j}\cdot\mathbf{r}} \tag{3}$$

The stimulated signal is defined as the change in the photon occupation number of the detected mode ω, belonging to the probe pulse E_s [Eq. (4)]:

$$S = \int_{-\infty}^{+\infty} dt \frac{d}{dt}\left\langle a_s^\dagger(t)a_s(t)\right\rangle = \frac{2}{\hbar}\int_{-\infty}^{\infty}\frac{d\omega'}{2\pi}\Im\left\langle P(\omega')\varepsilon^\dagger(\omega')\right\rangle \tag{4}$$

where [Eq. (5)]:

$$P(\omega) = \int_{-\infty}^{+\infty} dt\, e^{i\omega(t-T)}P(t) \tag{5}$$

and $P(t) = Tr[\alpha\rho(t)]$ is the nonlinear polarization induced by the pulses. The time derivative in Equation (4) is evaluated by using the Heisenberg equation of motion. The expectation value $\langle\ldots\rangle = Tr[\rho(t)\cdot\ldots]$ may be calculated by solving the density matrix for the total system $\rho(t)$, which includes both the radiation and matter degrees of freedom. This is easily achieved by working in the interaction picture. Moreover, the density matrix propagation is most compactly described by superoperators in Liouville space.[23,24] The stimulated optical signal obtained by a frequency gated measurement is then given by Equation (6):[25]

$$S(\omega,T) = \frac{2}{\hbar}\Im\mathcal{E}_s^*(\omega)\int_{-\infty}^{+\infty} dt\, e^{i\omega(t-T)}\left\langle \mathcal{T}P(t)e^{-\frac{i}{\hbar}\int_{-\infty}^{+\infty}dt'\,H'_-(t')}\right\rangle \tag{6}$$

where $\mathcal{T}$ is the time ordering superoperator and H'_- is the Liouville superoperator in the interaction picture. The detected field mode $\mathcal{E}_s^*(\omega)$ is selected by phase matching that is automatically guaranteed in the FSRS pulses configuration. The exponential in Equation (6) will be expanded in a power series and different orders can be accounted for using the loop diagrams.

Field interactions with matter are represented by arrows along the left and right branches of the loop. The two branches are not mutually time ordered, while interactions on the same branch are ordered. In the off-resonance regime, interactions with the fields are represented by pairs of arrows, an excitation to a virtual state followed to an instantaneous de-excitation to a real state.

3. FSRS Signals with Overlapping Pulses

The diagrams that contribute to the FSRS signal with electronically off-resonant pulses are shown in Figure 1. The FSRS signal is given by Equation (6). When the actinic pulse $\mathcal{E}_a$ and the probe pair, $\mathcal{E}_p$ and $\mathcal{E}_s$, are separated by a time interval longer than the pulse durations, the interaction Hamiltonian (1) becomes [Eq. (7)]:

$$H'(t) = \alpha(t)\left[\mathcal{E}_a^\dagger(t)\mathcal{E}_a(t) + \mathcal{E}_s^\dagger(t)\mathcal{E}_p(t)\right] + h.c. \tag{7}$$

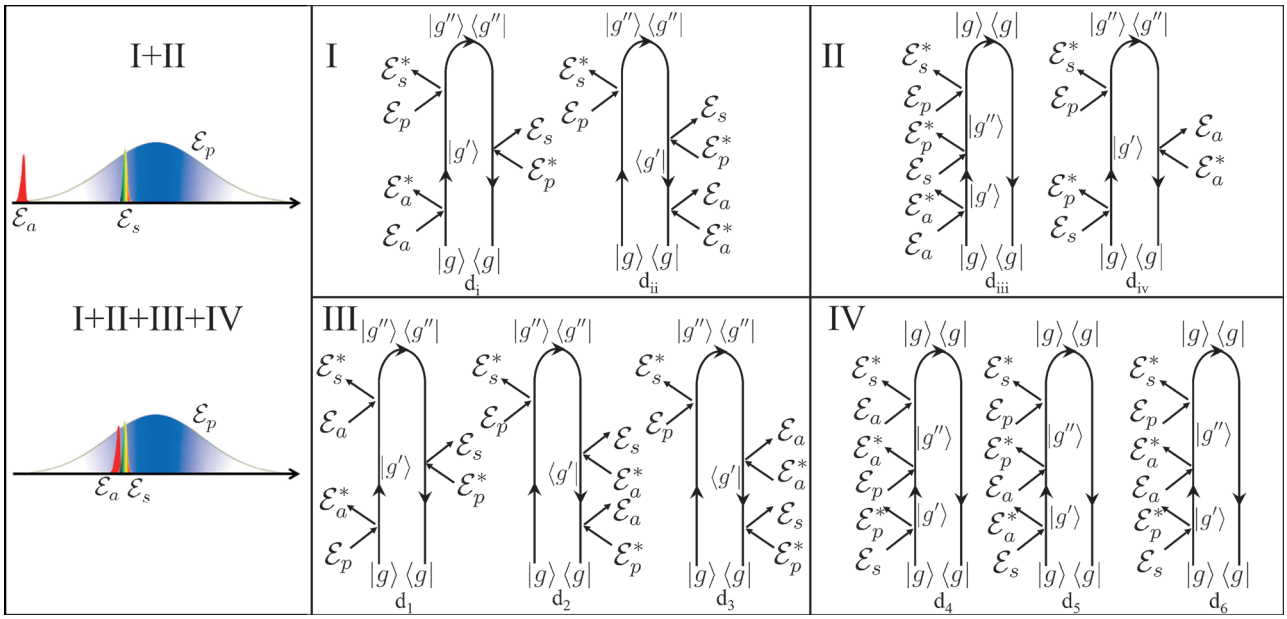

Figure 1. Pulse configuration and corresponding loop diagrams in off-resonance FSRS spectroscopy: In the conventional FSRS scheme, the actinic pulse triggers a photoinduced process and precedes a couple of Raman pulse and Raman probe fields. When the actinic does not overlap with the probe pulse, the total fifth-order signal is represented by four loop diagrams, two contributions (I) in the red side of the spectrum and two (II) on the blue side. However, when the dynamical process under investigation is exhausted in a timescale comparable to the ultrashort pulses duration, all fields are temporally overlapped, while the nonlinear signal is generated in the sample. In this case, six new contributions (III and IV) must be taken into account to calculate the fifth-order response of the system.

In diagrams d_i–d_{iv}, the first interaction is with the actinic field modes. Thus, they satisfy the pump–probe scheme and fully account for the pulse configuration shown on the top left side of the figure. In these diagrams, the off-resonant actinic pulse can either leave the system in the ground state or can impulsively trigger the excitation of low-frequency coherences. In the latter case, the $\mathcal{E}_s$ pulse probes higher frequency modes. Depending on the path involved, this physical process leads to the creation of main peaks at Raman frequencies as well as side peaks due to harmonic or anharmonic coupling between low and high frequency modes. These features evolve during the time delay T, from positive to negative and show dispersive lineshapes. In-depth analysis of these diagrams and the underlying of energy flow was given in our previous work.[26]

The most interesting case arises for time intervals in the overlap region, as sketched by the pulse configuration at the bottom of Figure 1: the number of diagrams increases and all the terms allowed by the summation in Equation (1) must to be taken into account.

We consider an actinic pulse with a spectrum centered on the red side of the Raman pulse. This choice determines the diagrams selection. Similar results can be obtained for an actinic pulse centered on the blue side. Taking all the possible permutations of the fields into account, we obtain three additional diagrams (d_1, d_2 and d_3) that contribute to the red side of the spectrum, that is, at frequencies lower than the central frequency of the $\mathcal{E}_p$ pulse, and three (d_4, d_5 and d_6) that give rise to features in the blue side.

Diagrams d_i–d_{iv} and d_1–d_6 involve two different vibrational modes to generate non-negligible signals. Remarkably, while diagrams d_i–d_{iv}, in addition to the probed mode, implicate a low-frequency mode covered within the bandwidth of the AP, on the other hand, diagrams d_1–d_6 require the presence of an extra level close to frequency difference between the RP and the AP.

The frequency dispersed FSRS signal $S_n(\omega,T)$ generated by diagram n can be easily evaluated in the frequency domain. We consider a three-level molecular system with a ground state g and two vibrational excited states, ω_1 and ω_2, with the higher close to the frequency difference between the Raman and the actinic pulse, $\omega_2=\omega_P-\omega_A$, being ω_P and ω_A the central frequency of RP and AP, respectively, and $\omega_1=800\ \mathrm{cm}^{-1}$. Simulations have been performed for a Gaussian actinic pulse centered at 650 nm and with a 50 fs FWHM and we assume a 490 nm monochromatic Raman pulse $\mathcal{E}_p(\omega) = 2\pi\, E_p\delta(\omega-\omega_P)$, which simplifies the frequency domain calculations.

We define the retarded Green's function [Eq. (8)]:

$$G(\omega) = \frac{1}{\hbar(\omega - H_0 + i\varepsilon)} = \frac{1}{\hbar}\sum_\alpha \frac{|\alpha\rangle\langle\alpha|}{\omega-\omega_\alpha+i\gamma} \tag{8}$$

and the advanced Green's function [Eq. (9)]:

$$G^\dagger(\omega) = \frac{1}{\hbar(\omega - H_0 - i\varepsilon)} = \frac{1}{\hbar}\sum_\alpha \frac{|\alpha\rangle\langle\alpha|}{\omega-\omega_\alpha-i\gamma} \tag{9}$$

where ε is a positive infinitesimal that ensures causality and further guarantees the convergence of the Fourier transform.

The right hand side of the equations is obtained by an expansion in the molecular eigenstate basis $|\alpha\rangle$ and γ is the vibrational dephasing rate.

Using the diagram rules[27] and Equation (6), we obtain for diagrams of Figure 1 [Eq. (10)]:

$$S_n(\omega,T) = (-1)^3 P_g \Im \int_{-\infty}^{+\infty} \frac{d\Delta_p}{2\pi}\frac{d\omega'_p}{2\pi}\frac{d\Delta}{2\pi}\frac{d\Delta_a}{2\pi}\frac{d\omega'_a}{2\pi}\, 2\pi\,\delta(\Delta_p-\Delta_a-\Delta)e^{-i\Delta_a T} \tag{10}$$
$$\mathcal{E}_p(\omega'_p)\mathcal{E}^*_p(\omega'_p+\Delta_p)\mathcal{E}_s(\omega+\Delta)\mathcal{E}^*_s(\omega)\mathcal{E}_a(\omega'_a+\Delta_a)\mathcal{E}^*_a(\omega'_a)F_n(\omega,\Delta,\Delta_p,\omega'_p,\Delta_a,\omega'_a)$$

where the correlation functions F_n depend on the diagram, as specified below, and T is the time delay between the $\mathcal{E}_s$ and $\mathcal{E}_a$ pulses; positive (negative) time delays imply that the actinic pulse precedes (follows) the probe pulse. Diagrams d_i–d_{iv} and d_1–d_6 contribute to the signal generated in the overlapping pulse configuration. The thermal occupation of the state (i) is accounted for through a Boltzmann factor $P_i = \left[1+e^{\beta(E_i-E_g)}\right]^{-1}$, with $\beta = 1/(k_B T)$, while the delta function provide energy conservation. The integration is performed on all the possible frequencies of the photons participating in the process, where the field $\mathcal{E}_k$ contributes with two photons, one of frequency ω_k and another of frequency $\omega_k+\Delta_k$.

The full response is given by the sum over all diagrams [Eq. (11)]:

$$S(\omega,T) = \sum_n S_n(\omega,T) \tag{11}$$

The correlation functions F_n contain the matter response and determine the signal lineshape and intensity. For diagrams d_i–d_{iv} we derive [Eqs.(12)–(15)]:

$$F_{d_i} = \left\langle \alpha G^\dagger(\omega'_p-\omega+\Delta_a)\alpha G(\Delta_a)\alpha\right\rangle \tag{12}$$

$$F_{d_{ii}} = \left\langle \alpha G^\dagger(\omega'_p-\omega)\alpha G^\dagger(\Delta-\Delta_p)\alpha\right\rangle \tag{13}$$

$$F_{d_{iii}} = \langle \alpha G(\Delta_a)\alpha G(\omega+\Delta-\omega'_p-\Delta_p+\Delta_a)\alpha\rangle \tag{14}$$

$$F_{d_{iv}} = \left\langle \alpha G^\dagger(\Delta-\Delta_p)\alpha G(\omega+\Delta-\omega'_p-\Delta_p)\alpha\right\rangle \tag{15}$$

while for the additional diagrams d_1–d_6 that contribute in the overlap configuration, we obtain [Eqs. (16)–(21)]:

$$F_{d_1} = \left\langle \alpha G^\dagger(\omega'_p-\omega'_a-\Delta_a)\alpha G(\omega'_p-\omega)\alpha\right\rangle \tag{16}$$

$$F_{d_2} = \left\langle \alpha G^\dagger(\omega'_p-\omega)\alpha G^\dagger(\omega'_p-\omega'_a-\Delta_a)\alpha\right\rangle \tag{17}$$

$$F_{d_3} = \left\langle \alpha G^\dagger(\omega'_p-\omega)\alpha G^\dagger(\omega'_p-\omega+\Delta_a)\alpha\right\rangle \tag{18}$$

$$F_{d_4} = \langle \alpha G(\omega-\omega'_a-\Delta_a)\alpha G(\omega-\omega'_p)\alpha\rangle \tag{19}$$

$$F_{d_5} = \langle \alpha G(\omega-\omega'_p)\alpha G(\omega-\omega'_a-\Delta_a)\alpha\rangle \tag{20}$$

$$F_{d_6} = \langle \alpha G(\omega-\omega'_p)\alpha G(\omega-\omega'_p-\Delta_a)\alpha\rangle \tag{21}$$

The correlation functions F_n depend on both the advanced and the retarded Green's functions, Equations (8) and (9).

Diagrams d_1 and d_4 are responsible for oscillating signals much broader than the typical vibrational linewidth ($\approx$10 cm^{-1}), since the last interaction couples the modes $\mathcal{E}_a$ and $\mathcal{E}_s^\dagger$, which does not allow for spectral resolution (spectral width of $\approx$300 cm^{-1}). Simulations carried for these diagrams by the sum over states are shown in Figure 2.

Only two diagrams for each side of the spectrum give additional sharp contributions to the Raman signal: diagrams d_2 and d_3 for the red side and diagrams d_5 and d_6 for the blue. These diagrams are responsible for signals that can be classified in two families. The first is characterized by a strong dispersive lineshape near $T=0$ that decays instantaneously outside an overlap region of the same size of the width of the actinic. This family includes diagrams d_2 and d_5 for the red and the blue side of the spectrum, respectively. The contributions of these diagrams around the overlap region $T=0$ are shown in the top panels of Figure 3. Outside this region, two-orders-of-magnitude-weaker features have been found, which evolve with T from dispersive to positive and negative features.

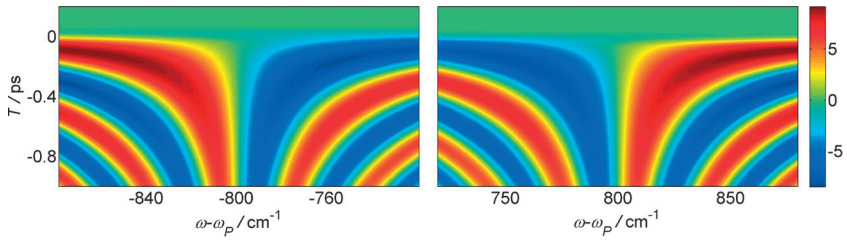

Figure 2. Additional contribution to fifth-order FSRS: A two-dimensional plot of fifth-order diagrams in the overlap region around $T=0$ and for $T<0$. Left panel: $S_{d_5}(\omega,T)$. Right panel: $S_{d_6}(\omega,T)$. These diagrams give rise to weak features for negative time delays, that is, when the probe pulse precedes the actinic pulse.

Diagrams d_3 and d_6 belong to the second family and similarly generate a dispersive feature in the overlap region but also non-negligible features at negative delays. These features appear as baseline oscillations on a dispersive signal. For positive time delays, small features oscillating with T have been found for this family as well. The contributions of diagrams d_3 and d_6 around the overlap region are shown in the bottom panels of Figure 3.

$S_{d_3}(\omega,T)$ and $S_{d_6}(\omega,T)$, displayed in Figure 4 for negative delays $T<0$, show baseline oscillations, with a period which is proportional to the time delay T. Such a behavior can be attributed to a gating effect due to the actinic pulse, which trun-

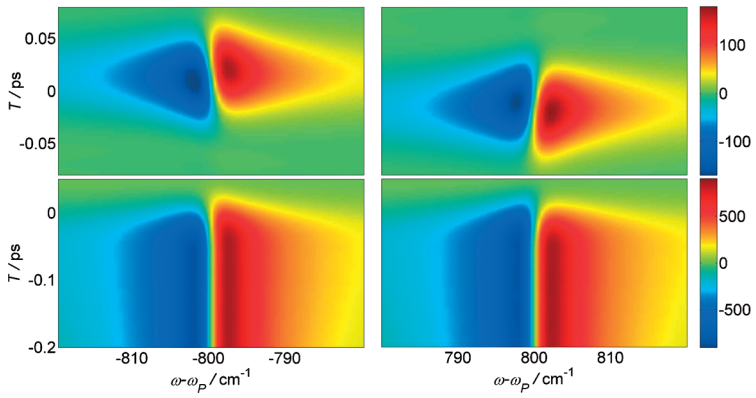

Figure 3. Fifth-order contributions for fully overlapping pulses or with the PP preceding the AP. Left panel: a two-dimensional plot of contributions from diagrams $S_{d_2}(\omega,T)$ (top) and $S_{d_3}(\omega,T)$ (bottom), which give rise to features in the red side of the spectrum. Right panel: a two-dimensional plot of contributions from diagrams $S_{d_5}(\omega,T)$ (top) and $S_{d_6}(\omega,T)$ (bottom), which are responsible for features in the blue side.

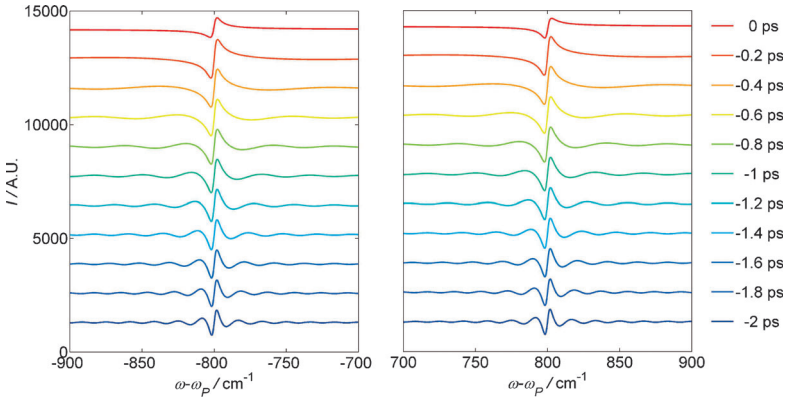

Figure 4. Fifth-order signal when the actinic pump comes after the probe pulse. $S_{d_5}(\omega,T)$ (left panel) and $S_{d_6}(\omega,T)$ (right panel) for negative delays T, with steps of 200 fs. For clarity, the traces are vertically offset.

cates the vibrational coherence. This result is particularly relevant since an oscillating behavior is also observed by 2D fifth-order experiments in the presence of anharmonic coupling.[28,29] Evaluating the relative magnitude of the two effects, which is strongly system-dependent, is beyond the scope of the present manuscript. However, an estimate of the weight of the fifth-order effect presented here, relative to the underlying stimulated Raman third-order response, can be derived from Equations 5.32 and 6.23 of Ref. [19] and it reads $P^{(5)}/P^{(3)} \approx \frac{|\mu_{ba}|^2|E_A|^2}{\hbar^2|\omega_A-\omega_{ba}||\gamma_{ca}|}$, which depends on the Actinic pump fluence and on the specific system of interest.

The $S_{d_3}(\omega,T)$ and $S_{d_6}(\omega,T)$ signals for $T<0$ are of the same order of magnitude of the total signal of fifth-order contributions during the overlap condition. Therefore, this pulse configuration can be used to directly calibrate the intensity of the fifth-order contribution. It has to be noted, however, that cross-phase modulation (XPM) between the actinic pump and the Raman pulse can generate competitive artifacts in the FSRS spectrum, especially for negative time delays.[30] A way to evaluate the magnitude of the P5 effect is to look at a secondary effect of the oscillating contributions at negative time delays, which generates an apparent decrease of the vibrational frequency of the third order response to the red side of the Raman pulse, as illustrated in Figure 4. Conversely, XPM at negative time delays induces a blue shift of the Raman pulse, that is, an increase of the apparent Raman shift is expected in the same spectral region. Consequently, an evaluation of the relative magnitude between P5 and XPM effects can be easily achieved by comparing the overall peak shift of the Raman bands at negative time delays.

The total signal $S_d(\omega,T)=\sum_{i=1}^{6} S_{d_i}(\omega,T)$, due to the additional diagrams d_1–d_6, is shown in the top panels of Figure 5. The weak features arising for positive values of T are analyzed in the insets. The case of a system with an additional low-frequency mode (50 cm^{-1} in this example) is reported in the bottom panels. Signals arise in such a case from the sum of diagrams d_i–d_{iv}, as it has been recently emphasized in Ref. [14].

4. Conclusions

We calculated fifth-order signals within the full overlap temporal region in FSRS experiments, for both the red and the blue side of the spectrum. The present description is based on loop diagrams, which take into account the propagation of the wave function forward and backward in time. The loop diagrams formalism differs from the conventional semi-classical approach because it treats both field and matter quantum-mechanically and allows us to significantly reduce the total number of diagrams in the expansion of the non-linear fifth-order signals.

We demonstrated that in the FSRS experiments, even in the absence of photoinduced dynamics, the pulse-overlap condition can generate time-dependent features. In particular, in the off-resonance regime, additional diagrams have to be considered when the overlap region is investigated. These contributions are superimposed to the predominant third-order signal, due to the action of the Raman and probe pulses solely, and can interfere with the time-resolved Raman spectrum.

The new contributions require, in addition to the probed vibrational mode, the presence of an additional vibrational level, whose frequency determines the pathways involved in the fifth-order process.

The most intuitive case is described by diagrams d_i–d_{iv} (Figure 1) and occurs for a low-frequency mode, in which the actinic pulse induces a coherence. Remarkably, in a more interesting situation, the extra vibrational level matches the RP and AP frequency difference, enabling pathways depicted in d_1–d_6 diagrams. While diagrams d_1 and d_4 generate broad signals, diagrams d_2 and d_3 give a sharp contribution on the red side

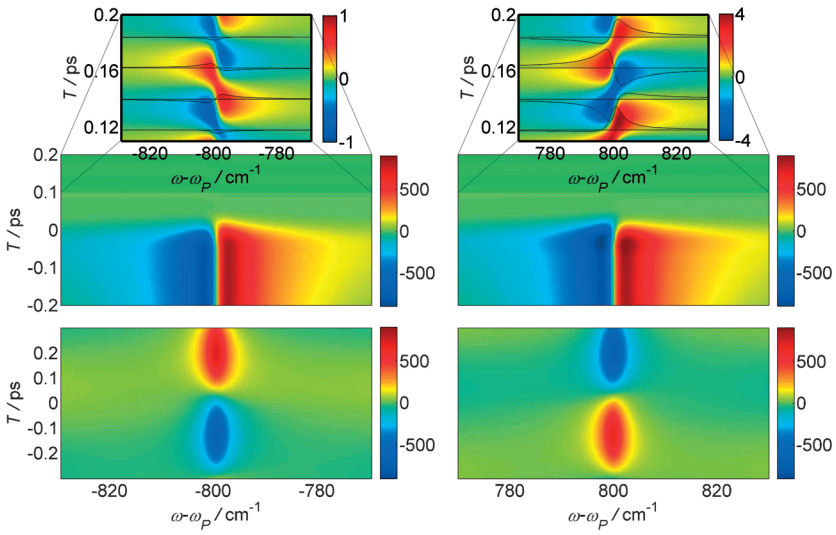

Figure 5. Total fifth-order signal: The total signal $S(\omega,T)$ for the red (left panel) and the blue (right panel) side of the spectrum, occurring when a vibrational level matching the RP and AP frequency difference is involved, is obtained summing the contributions from diagrams d_1,d_2,d_3 and d_4,d_5,d_6 respectively. The insets represent a magnification of the total signal for positive T, in order to emphasize weak temporal oscillating contributions, surviving outside the overlap condition. The bottom panels show the total signal $S(\omega,T)$ for a system with a low-frequency mode at 50 cm^{-1} (not included in the top panels), arising from the sum of diagrams d_i–d_{ii} (red side) and d_{iii}–d_{iv} (blue side).

and diagrams d_5 and d_6 give a sharp contribution on the blue one. Moreover, we found that even when the actinic pulse is delayed relative to the probe pulse, diagrams d_3 and d_6 give a substantial contribution (Figure 4) which can be used as a easy detectable benchmark of the total fifth order processes intensity. Our work raises a fundamental issue for the detection of a wavepacket motion by pushing FSRS towards its time resolution limit. Real dynamics might indeed be obscured by unwanted non linear effects, arising by the increasing complexity of the time ordering ruling the FSRS process once the pump and probe pulses are no longer well separated.

Acknowledgements

S.M. is grateful for the hospitality and support while at the Universitá di Roma "Sapienza" as a Visiting Professor and gratefully acknowledges the support of the National Science Foundation through Grant No. CHE-1361516, and the Chemical Sciences, Geosciences and Biosciences Division, Office of Basic Energy Sciences, Office of Science, U.S. Department of Energy.

Keywords: femtochemistry · nonlinear optics · pump–probe spectroscopy · Raman spectroscopy · time-resolved spectroscopy

[1] H. Hamaguchi, T. L. Gustafson, *Annu. Rev. Phys. Chem.* **1994**, *45*, 593 – 622.
[2] Y. Mizutani, T. Kitagawa, *Science* **1997**, *278*, 443 – 446.
[3] P. Kukura, D. W. McCamant, R. A. Mathies, *Annu. Rev. Phys. Chem.* **2007**, *58*, 461 – 488.
[4] M. Yoshizawa, Y. Hattori, T. Kobayashi, *Phys. Rev. B* **1994**, *49*, 13259 – 13262.
[5] D. W. McCamant, P. Kukura, S. Yoon, R. A. Mathies, *Rev. Sci. Instrum.* **2004**, *75*, 4971 – 4980.
[6] C. Fang, R. R. Frontiera, R. Tran, R. A. Mathies, *Nature* **2009**, *462*, 200 – 204.
[7] A. L. Dobryakov, I. Ioffe, A. A. Granovsky, N. P. Ernsting, S. A. Kovalenko, *J. Chem. Phys.* **2012**, *137*, 244505.
[8] H. Kuramochi, S. Takeuchi, T. Tahara, *J. Phys. Chem. Lett.* **2012**, *3*, 2025 – 2029.
[9] E. Pontecorvo, C. Ferrante, C. G. Elles, T. Scopigno, *J. Phys. Chem. B* **2014**, *118*, 6915 – 6921.
[10] E. Pontecorvo, S. M. Kapetanaki, M. Badioli, D. Brida, M. Marangoni, G. Cerullo, T. Scopigno, *Opt. Express* **2011**, *19*, 1107 – 1112.
[11] E. Pontecorvo, C. Ferrante, C. G. Elles, T. Scopigno, *Opt. Express* **2013**, *21*, 6866 – 6872.
[12] D. P. Ho man, D. Valley, S. R. Ellis, M. Creelman, R. A. Mathies, *Opt. Express* **2013**, *21*, 21685.
[13] P. Kukura, D. W. McCamant, S. Yoon, D. B. Wandschneider, R. A. Mathies, *Science* **2005**, *310*, 1006 – 1009.
[14] S. Mukamel, J. D. Biggs, *J. Chem. Phys.* **2011**, *134*, 161101.
[15] D. W. McCamant, P. Kukura, R. A. Mathies, *Appl. Spectrosc.* **2003**, *57*, 1317 – 1323.
[16] S. Y. Lee, S. Yoon, R. A. Mathies, *J. Phys. Conf. Ser.* **2006**, *28*, 36 – 41.
[17] B. P. Fingerhut, K. E. Dorfman, S. Mukamel, *J. Chem. Theory Comput.* **2014**, *10*, 1172 – 1188.
[18] D. W. McCamant, *J. Phys. Chem. B* **2011**, *115*, 9299 – 9305.
[19] S. Mukamel, *Principles of Nonlinear Optical Spectroscopy*, Oxford University Press, Oxford, **1995**.
[20] F. Provencher, N. Bérubé, A. W. Parker, G. M. Greetham, M. Towrie, C. Hellmann, M. Côté, N. Stingelin, C. Silva, S. C. Hayes, *Nat. Commun.* **2014**, *5*, 4288.
[21] K. E. Dorfman, B. P. Fingerhut, S. Mukamel, *Phys. Chem. Chem. Phys.* **2013**, *15*, 12348.
[22] S. Rahav, S. Mukamel, *Adv. At. Mol. Opt. Phys.* **2010**, *59*, 223 – 263.
[23] U. Harbola, S. Mukamel, *Phys. Rep.* **2008**, *465*, 191 – 222.
[24] S. Mukamel, *Phys. Rev. E* **2003**, *68*, 021111.
[25] K. E. Dorfman, B. P. Fingerhut, S. Mukamel, *J. Chem. Phys.* **2013**, *139*, 124113.
[26] G. Batignani, G. Fumero, S. Mukamel, T. Scopigno, *Phys. Chem. Chem. Phys.* **2015**, *17*, 10454 – 10461.
[27] J. D. Biggs, J. A. Voll, S. Mukamel, *Philos. Trans. R. Soc. A* **2012**, *370*, 3709 – 3727.
[28] D. T. Valley, D. P. Ho man, R. A. Mathies, *Phys. Chem. Chem. Phys.* **2015**, *17*, 9231 – 9240.
[29] D. P. Hoffman, S. R. Ellis, R. A. Mathies, *J. Phys. Chem. A* **2014**, *118*, 4955 – 4965.
[30] G. P. Agrawal, P. L. Baldeck, R. R. Alfano, *Phys. Rev. A* **1989**, *40*, 5063 – 5072.

Manuscript received: June 9, 2015
Accepted Article published: September 21, 2015
Final Article published: ■■ ■■, 0000

ARTICLES

Overlaying signals: Assessing the resolution limit of pump–probe spectroscopies is a critical issue for tackling ultrafast phenomena. The authors address the case of femtosecond stimulated Raman spectroscopy under the extreme condition of time overlap between the pulses initiating the photoexcitation and those probing the subsequent dynamics. Surprisingly, new time-dependent features originate affecting the signal resolution.

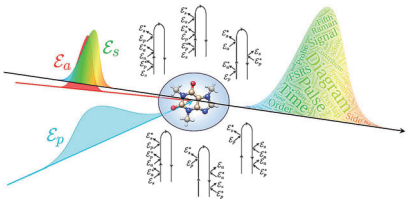

*G. Fumero, G. Batignani, K. E. Dorfman, S. Mukamel, T. Scopigno**

■■ – ■■

On the Resolution Limit of Femtosecond Stimulated Raman Spectroscopy: Modelling Fifth-Order Signals with Overlapping Pulses

These are not the final page numbers! ↗↗